Hopping conduction in partially compensated doped silicon

J. Zhang, W. Cui, M. Juda, and D. McCammon
Department of Physics, University of Wisconsin, Madison, Wisconsin 53706

R. L. Kelley, S. H. Moseley, C. K. Stahle, and A. E. Szymkowiak
NASA/Goddard Space Flight Center, Greenbelt, Maryland 20771
(Received 17 March 1993)

We have measured the dc electrical resistance of partially compensated (5–50 %) ion-implanted Si:P,B (both n and p type), over the temperature range 0.05–30 K. The temperature behavior is consistent with the prediction of the model for variable-range hopping (VRH) with a Coulomb gap $\rho(T)=\rho_0\exp(T_0/T)^{1/2}$ over a temperature range $6.5<T_0/T<24$. We observe deviations from this behavior at our high- and low-temperature extremes. In the low-temperature region, the resistivities show a stronger temperature dependence than the Coulomb-gap model prediction. The high-temperature deviation appears consistent with a transition from Coulomb-gap VRH to Mott VRH.

I. INTRODUCTION

The measurements described below were undertaken as part of an empirical program to characterize semiconductor thermistors as thermometers for high-resolution single-quantum calorimeters. The theory of operation of these cryogenic microcalorimeters has been described elsewhere.[1–4] Interest in their development as a new type of spectroscopic detector stems largely from their promise of more than two orders of magnitude improvement in energy resolution over conventional Si(Li) detectors. We chose semiconductor thermistors operating in the hopping conduction regime as the thermometer element based on their long history of use in infrared bolometers, where they have been assumed to operate as ideal resistive thermometers,[5] and because fabrication techniques exist that make it easy to integrate them into the detector structure.[4,6]

We have currently achieved a resolution of 7.3 eV full width at half maximum for 6-keV x rays.[7] Further improvement of the energy resolution requires reducing the detector operating temperature and heat capacity (and therefore the volume of the heavily doped thermistor with its relatively large specific heat) while maintaining a high thermometer sensitivity.

We discovered that these requirements conflict: reducing the volume of the thermistor causes an electrical nonlinearity that spoils its temperature sensitivity long before technological limits on its size are reached.[8] This problem becomes rapidly worse as the temperature is lowered, and the onset of electrical nonlinearity occurs earlier (at higher temperatures and larger volumes) for thermistors with higher intrinsic sensitivity. The thermistors also exhibit excess noise under bias that is worse for lower operating temperature, smaller volumes, and higher sensitivity.[8] These effects make the thermistor a major limitation on the achievable energy resolution, and it is clear that at least an empirical understanding of the behavior of the thermistors is needed in order to optimize the design of detectors.

The electrical nonlinearity and excess noise will be discussed elsewhere.[9] In this paper, we report on the behavior of the conductivity of doped silicon in the limit of small fields, where the current is proportional to the applied voltage. Since this investigation was part of an x-ray detector development program, the types of samples used and range of measurement parameters were not optimum for a study of the basic physics, nor could we justify doing some fairly obvious follow-up experiments. However, the data we obtained are of good quality and cover a wide range of doping density at moderate compensation. They offer the clearest evidence yet for the existence of a Coulomb gap[10] in doped silicon, but show systematic deviations from this behavior at the high- and low-temperature extremes of our measurements.

Theoretical studies of charge transport in doped semiconductors at low temperatures have shown that on the insulator side of the metal-insulator transition, thermally activated tunneling between impurity sites is the dominant conduction mechanism.[10–13] These theories predict that the resistivity has a temperature dependence

$$\rho(T)=\rho_0\exp(T_0/T)^p\ . \tag{1}$$

The nearest-neighbor hopping model,[11] where tunneling occurs to the nearest accessible sites, predicts that the exponent $p=1$. Mott suggested that as the temperature is lowered, competition between the $e^{-l/a}$ tunneling term, where l is the hopping distance and a is the electron localization radius, and the $e^{-\Delta E/kT}$ activation term makes it more favorable for an electron to hop to increasingly more distant sites, with smaller ΔE, rather than to the nearest neighboring site.[12] This is called variable-range hopping (VRH). In this case, if the density of states (DOS) around the Fermi level is approximately constant, $p=\frac{1}{4}$ for a three-dimensional (3D) system (the Mott law), and $p=\frac{1}{3}$ for a 2D system. Efros and Shklovskii subsequently proposed that if long-range Coulomb interactions between localized electrons are considered, the DOS should go to zero quadratically at the Fermi level for a

0163-1829/93/48(4)/2312(8)/$06.00

TABLE I. Ion-implant schedules for 3.4×10^{18} cm^{-3} net doping density and 50% compensation.

n type				*p* type			
Phosphorus		Boron		Phosphorus		Boron	
Energy (keV)	Dose (cm^{-2})	Energy (keV)	Dose (cm^{-2})	Energy (keV)	Dose (cm^{-2})	Energy (keV)	Dose (cm^{-2})
93.4	3.84×10^{13}	27.4	1.70×10^{13}	65.1	1.14×10^{13}	27.0	2.86×10^{13}
153.6	6.83×10^{13}	47.9	2.57×10^{13}	100.5	1.79×10^{13}	43.9	4.25×10^{13}
274.8	1.60×10^{14}	82.1	3.93×10^{13}	157.4	3.29×10^{13}	72.1	6.81×10^{13}
		142.1	6.39×10^{13}	275.9	7.87×10^{13}	124.9	1.19×10^{14}

3D system, resulting in an exponent $p=\frac{1}{2}$ (the "Coulomb-gap" model).[10] For VRH in general, if the DOS has the energy dependence $g(\varepsilon)\propto\varepsilon^m$, where ε is the energy measured from the Fermi level, the parameter p in Eq. (1) is given by

$$p=\frac{m+1}{m+1+d}\ , \tag{2}$$

where d is the dimensionality of the system.[13,14] With the Coulomb interaction, $m=1$ for a 2D system and $m=0$ for a 1D system, resulting in $p=\frac{1}{2}$ for all dimensions.

Many experimental studies have been devoted to investigating hopping conduction in doped germanium and silicon. Mott behavior $\rho=\rho_0'\exp(T_0'/T)^{1/4}$ was observed in germanium by Allen and Adkins over a wide range of temperatures.[15] Evidence for the Coulomb-gap behavior $\rho=\rho_0\exp(T_0/T)^{1/2}$ was later reported in doped Ge.[16–20] Most studies of doped Si have used uncompensated samples. The Mott law fits much of these data over a wide temperature range, although some data show a stronger temperature dependence at very low temperatures.[21–23] Some evidence has been found for $p=\frac{1}{2}$ behavior in thin ion-implanted samples[6,24,25] and over the relatively narrow temperature range 1–4 K in a bulk sample.[26] Few data have been published for moderately compensated silicon over a wide range of temperature, and it does not show conclusive evidence for any particular temperature dependence.[27]

II. SAMPLE PREPARATION AND MEASUREMENT

Selectively doping a small volume of silicon by ion implantation provides a suitable technique for making thermometers for monolithic microcalorimeters, and the samples tested here were prepared with the same processing steps as we use for detector fabrication. The processing sequence is outlined in the appendix. Both 100 Ω cm *p*-type float zone and 40 Ω cm *n*-type Czochralski ⟨100⟩ wafers were used as the starting material with no discernible difference in the low-temperature behavior of the devices.

Table I gives the implant schedules for 50% compensation and 3.4×10^{18} cm^{-3} net doping density. Other doping densities and compensations are simply scaled from these. The impurity ions were implanted at several different energies to get reasonably flat-topped depth profiles. Figure 1 shows the calculated net density and compensation profiles versus depth for these schedules, including the effects of diffusion during the annealing cycle. We made the minority dopant depth profile slightly wider than that of the majority dopant to avoid possible degeneracy at the front and back surface of the implant due to undercompensation caused by differential diffusion of the dopants. Some early *n*-type devices showed a flattening of the resistance at low temperature that appeared to be due to degenerate shunts along the edges of the implant caused by lateral diffusion of the boron. We eliminated this problem by etching 10 μm wide×8 μm deep trenches along the edges of the implant to remove the degenerate material.

The test devices were made in sizes ranging from 25×25 μm^2 to 400×400 μm^2, with length to width ratios between 10:1 and 1:10, and in both *n*-type and *p*-type devices so that we could check for size, geometry, or carrier-type dependences. Most devices had 50% compensation, but a few samples were prepared with 5% compensation for comparison. Degenerate contacts overlapping the ends of the devices and extending across their full width were implanted according to the schedules in

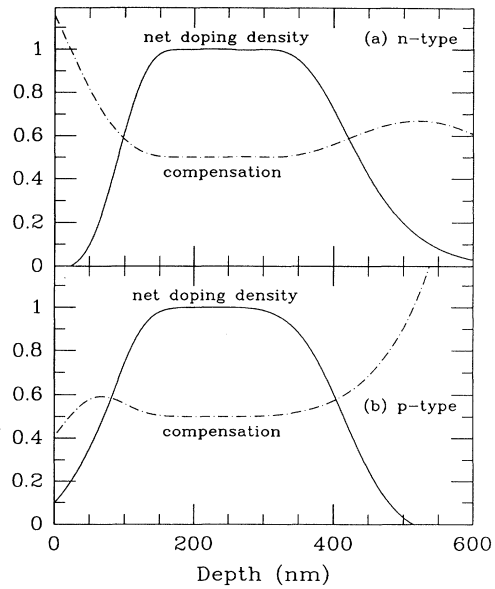

FIG. 1. Solid lines are the normalized net doping density as a function of depth for our ion-implanted samples, including the effects of diffusion during annealing. The dashed lines are the compensation level (a) *n*-type implants, (b) *p*-type implants. The implant schedules are listed in Table I.

TABLE II. Contact implant schedules.

n type				*p* type	
Phosphorus		Arsenic		Boron	
Energy (keV)	Dose (cm^{-2})	Energy (keV)	Dose (cm^{-2})	Energy (keV)	Dose (cm^{-2})
93.4	3.84×10^{13}	27.4	1.70×10^{13}	100.0	1.50×10^{15}
153.4	6.83×10^{13}	47.9	2.57×10^{13}		

Table II. Careful measurements on test structures containing twenty pairs of metal-contact or contact-thermistor connections in series show negligible barrier resistance at currents as low as a few picoamperes.

The low-temperature conductivity of doped semiconductors is a very steep function of the doping density, so we took considerable care to ensure uniform and repeatable implants. The wafers were tilted by 7.5° from normal to the incident ion beam around an axis 14° from ⟨110⟩, following the standard practice to minimize ion channeling along the crystal axes. We estimated that the implanted dose should be uniform and repeatable to 1% across the 3-in. wafers, but we consistently found gradients in the low-temperature resistivity across a wafer that corresponded to ~15% changes in the effective doping density. The only explanation we have for this effect is the seemingly remote possibility that the ~3° change in the angle of the incident ion beam as it scans across the wafer affects ion channeling enough to alter the depth profile significantly. The problem was minimized by spinning the wafers about the ⟨100⟩ normal at ~300 rpm during implantation. This reduced the nonuniformity to a small radial gradient. Even without spinning, there was no small-scale structure in the variations, and devices within a few millimeters of each other on the wafer always had virtually identical properties.

We note that there seems to be no way to determine the low-temperature properties from room-temperature behavior. Room-temperature resistivity variations are quite small, and in some case where we mapped resistance of devices over an entire wafer at both 300 and 0.1 K, the two sets of contours were almost orthogonal.

Dice containing several devices were cut from the wafers and epoxied onto TO-5 transistor headers, which were then clamped to the cold plate of a ^{3}He cryostat or adiabatic demagnetization refrigerator (ADR). A Faraday cage and rf filters were used to avoid radio-frequency pickup. We found no effect due to the small (< 10 G) magnetic field on samples in the ADR.

Temperatures were measured with calibrated germanium resistance thermometers (Lake Shore Cryotronics) for 0.05 K < T < 20 K, and with a calibrated GaAlAs diode (also Lake Shore Cryotronics) for T > 20 K. For the low-temperature range, we compared thermometers from different lots, and found agreement to ~1 mK. Sample resistance was measured using a Keithley model 616 electrometer to monitor the current and a voltage amplifier to measure the voltage. At each cold plate temperature, we applied a range of currents, plotted resistance versus power dissipated, and checked that the resistance goes to a constant limiting value as the power goes to zero. The drop in resistance with increasing power shown in Fig. 2 is almost entirely due to an intrinsic nonlinearity of the resistor and not to heating of the die.[9]

We note here that while the ion-implanted silicon samples consistently display the type of low-temperature behavior discussed in the following sections, our experience with melt-doped silicon and germanium (at least at these intermediate compensation levels) has been that many samples curve downward in resistance relative to implanted silicon or neutron-transmutation-doped germanium at the lowest temperatures. They also become nonlinear at considerably smaller electric fields. Both of these behaviors are consistent with the presence of small-scale nonuniformities in the doping density.

III. EXPERIMENTAL RESULTS

Figure 3 shows the dc electrical resistivities in the low-field limit as a function of $T^{-1/2}$ for seven 50% compensated ion-implanted samples. With the exception of the most heavily doped sample, no. 1, all of the devices fall on straight lines over a considerable range of resistance, showing the $p=\frac{1}{2}$ behavior expected from the Coulomb-gap model. Since there are deviations from this behavior at both low and high temperatures for most of the samples, we fit all of them to a $\rho=\rho_0\exp(T_0/T)^{1/2}$ model over the same temperature range relative to the characteristic temperature T_0. The range $6.5 < T_0/T < 24$ was chosen since all samples except no. 1 appear to fit the ex-

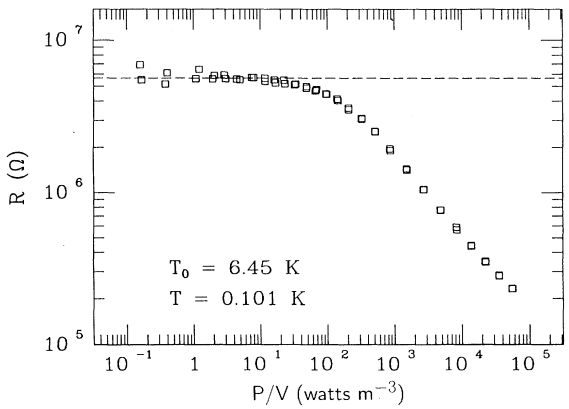

FIG. 2. Example of resistance vs applied power. The dashed line shows the derived zero-field limiting value used in the analysis. The resistance drop at high powers is due to intrinsic nonlinearity and not to heating of the die.

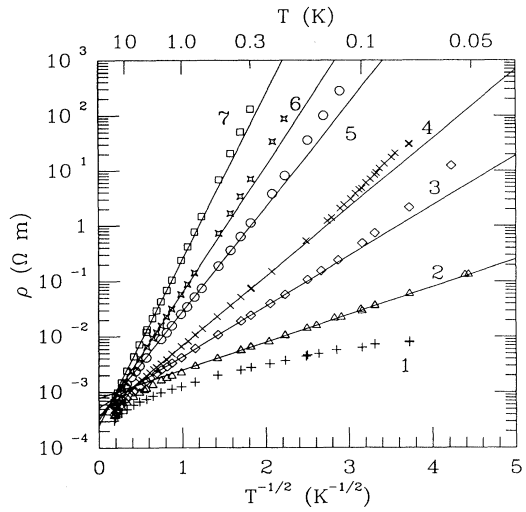

FIG. 3. Resistivity vs $T^{-1/2}$ for seven ion-implanted Si:P,B samples with 50% compensation. The straight lines are fits to the Coulomb-gap model, $\rho=\rho_0\exp(T_0/T)^{1/2}$, over a temperature range of $6.5<T_0/T<24$. Sample 1 does not fit this model over any part of the measured temperature range.

pression well over this interval. The fits were iterated a few times to ensure that T_0 converged to a constant value. Table III lists the resulting best-fit values of T_0 and ρ_0.

We have replotted the resistivity data divided by the best fit $p=\frac{1}{2}$ model against the reduced inverse temperature T_0/T in Fig. 4. The greatly expanded scale shows how good the fits are and shows the systematics of their deviations at low and high temperatures. The $p=\frac{1}{2}$ behavior holds for almost the same range of reduced temperature for all samples, whereas there are large changes in the actual temperature range.

It is notoriously difficult to determine power law slopes accurately when they are valid only over a limited range. As a test of how precisely the data fix the slope at $\frac{1}{2}$, we generated two artificial data sets that followed $p=0.4$ and 0.6 in Eq. (1) instead of $p=\frac{1}{2}$. These artificial data were fit to a $p=\frac{1}{2}$ model using the same procedure as the real data fits. We adjusted ρ_0'' and T_0'' used to generate the artificial data (with $p=0.4$ and 0.6) to give the same fit values of ρ_0 and T_0 (for $p=\frac{1}{2}$) as those of sample 4. The two artificial data sets and the real data from sample 4 were all divided by this same best fit $p=\frac{1}{2}$ model and plotted together in Fig. 5. Sample 4 clearly follows an intermediate slope over a finite range of temperature with reasonably sharp transitions to shallower and steeper temperature dependence at lower and higher temperatures, respectively.

The effects of carrier type and compensation are illustrated in Fig. 6, where data for devices with similar T_0's are compared. There is no significant difference between the n-type and p-type samples. Devices with 5% and 50% compensation follow the Coulomb-gap model over approximately the same temperature range, but they behave somewhat differently at low and high temperatures.

Figure 7 shows derived T_0's as a function of the doping densities estimated from integrating the ion current during implantation. We fit the data with a function of the form $T_0=\Theta(1-n/n_c)^{\eta}$, which is taken from Ref. 13 (p. 242). As discussed in Sec. II, there is a large scatter in T_0 for identical implants; as a consequence, our data cannot constrain the value of η within the expected range[28] of 2.0–2.5. The lines in Fig. 7 are from the least-squares fits with η fixed at 2.0. One can see, however, that p-type samples require higher net doping densities than n-type samples to get the same T_0. Figure 8 shows the relationship between ρ_0 and T_0 for a variety of devices.

IV. DISCUSSION

We find that the model of variable range hopping with a Coulomb gap $\rho=\rho_0\exp(T_0/T)^{1/2}$ fits our moderately compensated ion-implanted silicon samples over the temperature range $6.5<T_0/T<24$. Even though T_0 varies considerably for implants that we think should have almost identical doping densities, this one characteristic temperature seems to completely determine the low-temperature properties of a device. As shown in Fig. 8, ρ_0 can be predicted quite accurately from T_0, independent of carrier type or compensation. Figure 6 shows that the deviations from Coulomb-gap behavior are also independent of carrier type, although they are affected somewhat by the compensation level. Nonlinearity effects at all power levels also appear to be determined by T_0 alone.[9]

We have observed deviations from the Coulomb-gap prediction at both high and low temperatures. The steeper temperature dependence at low temperature is

TABLE III. A summary of model fitting parameters. T_0 and ρ_0 are parameters for Coulomb gap model, and T_0' and ρ_0' are for the Mott law.

Sample	Type	N_{net} (cm^{-3})	T_0 (K)	ρ_0 (Ω cm)	T_0' (K)	ρ_0' (Ω cm)
1	p	5.61×10^{18}			21.3	1.50×10^{-2}
2	n	4.25×10^{18}	1.36	7.65×10^{-2}	152	8.41×10^{-3}
3	n	4.25×10^{18}	4.40	5.29×10^{-2}	310	6.73×10^{-3}
4	p	4.76×10^{18}	8.29	3.82×10^{-2}	437	6.11×10^{-3}
5	n	3.57×10^{18}	18.9	3.44×10^{-2}	1390	4.08×10^{-3}
6	n	3.57×10^{18}	27.9	3.10×10^{-2}	2459	2.88×10^{-3}
7	n	3.23×10^{18}	47.5	2.47×10^{-2}	5168	1.78×10^{-3}

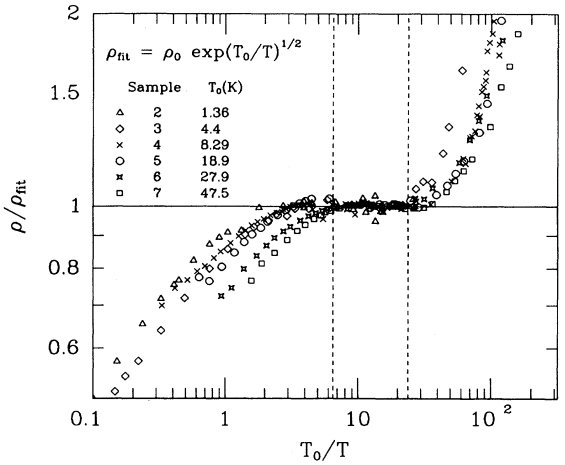

FIG. 4. Resistivity of samples 2–7 divided by the best fit $p=\frac{1}{2}$ model of samples 2–7 vs the reduced inverse temperature T_0/T. Symbols are the same as in Fig. 3.

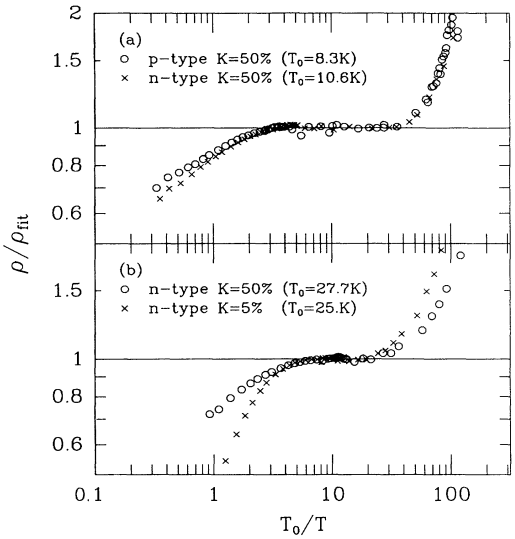

FIG. 6. (a) Comparison of a p-type sample and an n-type sample with similar T_0's. (b) Comparison of n-type samples with 5% and 50% compensation, but similar T_0's.

difficult to explain as a measurement artifact. The only experimental difficulty that could cause this would be inhomogeneity of the doping density along the sample length. In this case, we should have seen a larger effect for long and narrow samples; in fact we found no difference between samples with 6:1 and 1:6 geometries. Other experimental factors, such as self-heating, rf pick-up, or other parasitic heat loads, result in the opposite curvature.

One plausible explanation for the steeper temperature dependence at low temperature is the onset of finite thickness effects in our thin (~2000 Å) samples. In the percolation model discussed by Shklovskii and Efros (see Ref. 13, Sec. 5.6) continuous conductive networks first form when hops of length up to $r_c = a\xi_c$ are included, where a is the electron localization length and $\xi_c \approx (T_0/T)^{1/2}$, since these longest hops dominate the resistivity. The porosity scale of the conductive network is described by a correlation length L equal to $r_c\xi_c^{\nu}$. Since $\nu \approx 1$, $L \approx a\ (T_0/T)$. If the thickness of the sample approaches the correlation length, the surfaces begin to interrupt a large fraction of the conductive links, and the resistivity will increase exponentially as the thickness is further decreased (see Ref. 13, Sec. 9.3). If we assume that the resistivity is increased by a factor of $\sim e$ when the thickness is just equal to the correlation length, we can see from Fig. 4 that this happens for T_0/T between 60 and 160 for our samples. This implies localization lengths ranging from 13 Å for the more lightly doped samples to 33 Å for the more heavily doped. Although we cannot determine the localization lengths directly,

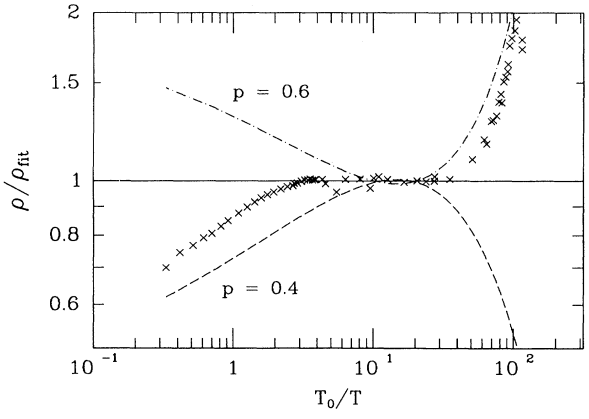

FIG. 5. Comparison of the data for sample 4 with two artificial data sets that actually follow $\rho_0''\exp(T_0''/T)^p$, with $p=0.4$ and 0.6. This allows an estimate of the precision with which the exponent p is determined by the experimental data. See text for discussion.

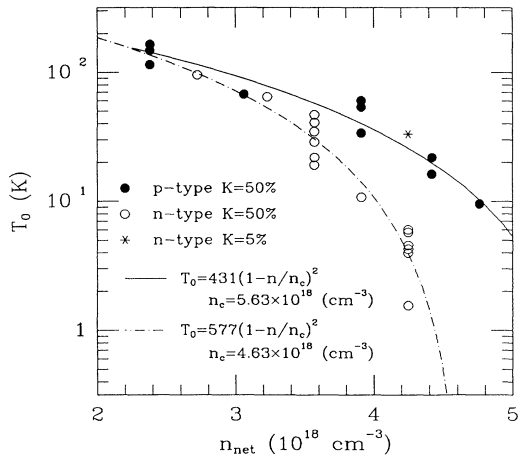

FIG. 7. T_0 for the Coulomb-gap model vs n_{net}, the net impurity density for our n-type and p-type ion-implanted Si:P,B samples. The functional form of the fits is from Ref. 13 (p. 242).

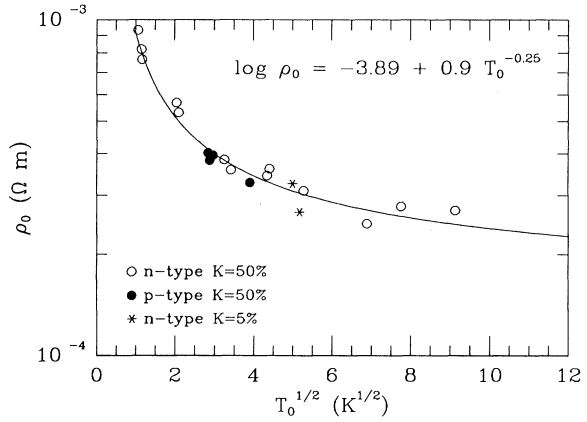

FIG. 8. ρ_0 vs $\sqrt{T_0}$ for the Coulomb-gap model. The solid line is an empirical fit.

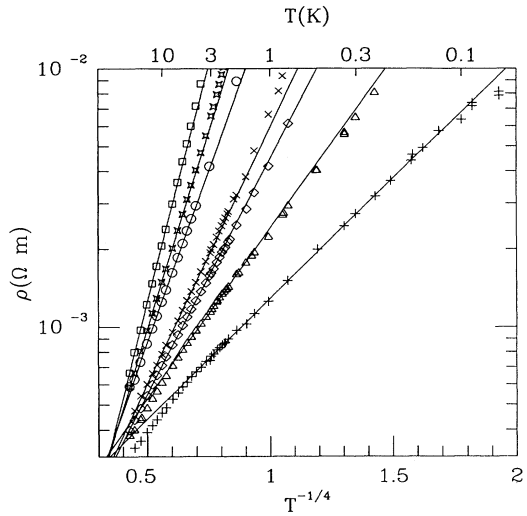

FIG. 9. $\rho(T)$ vs $T^{-1/4}$ for the samples shown in Fig. 3. The high-temperature data have been fit with the Mott law model: $\rho=\rho_0'\exp(T_0'/T)^{1/4}$. The best-fit values of the parameters T_0' and ρ_0' are listed in Table III.

these values lie between the radius of the electron wave function of isolated impurities (~13 Å) and the mean impurity spacing (~65 Å).

As a check on the possibility of a thickness effect, we have performed a crude experiment in which we etched away about half the 2000 Å thickness of two implanted samples with a NF_3/Ar reactive ion etch. The $R(T)=R_0\exp(T_0/T)^{1/2}$ behavior persisted after this thinning, but rather than the expected result that T_0 should stay the same and R_0 be approximately doubled, we found that R_0 remained about the same while T_0 increased significantly. This appears to support the conclusion that the conduction is not fully three dimensional, but we hesitate to give much weight to this result, since the surface of the implant was exposed and heavily contaminated by the ion etch, with unknown effects on the conductivity.

Another possible explanation for the steeper temperature dependence at low temperature was first proposed by Shlimak, who observed similar behavior in a ^{74}Ge(As) sample and suggested that a magnetic hard gap due to spin-spin interaction might be responsible for this stronger temperature dependence in resistivity at low temperatures.[29] Shlimak's suggestion has since been used to explain the low-temperature behavior of ion-implanted Si:As (Ref. 30) and bulk-doped Si:B.[31] Van der Heijden *et al.* dismiss the possibility of finite thickness effects in their ion-implanted samples, assuming (incorrectly, we believe) that these should flatten rather than steepen the temperature dependence.[30] Dai, Zhang, and Sarachik, on the other hand, showed that when magnetic fields > 1 T are applied to their bulk-doped Si:B samples, the resistivity reverts to the Coulomb gap form, providing evidence that the steeper behavior was indeed a magnetic effect.[31]

In the high-temperature region our data appear to fit the Mott law, as shown in Fig. 9. The best-fit values of the parameters T_0' and ρ_0' are listed in Table III. We expect that the $p=\frac{1}{2}$ behavior predicted for systems with a Coulomb gap in the density of states should be observed only so long as the typical hopping energy is less than the width of the gap. Castner estimated[32] that the transition from $p=\frac{1}{4}$ to $\frac{1}{2}$ occurs at $T\approx T_0/25$ for samples with compensation level $K\ll 1$. Because the Coulomb-gap width increases rapidly with compensation level [it is expected to vary as $K^{1/3}(1-K)^{1/3}$; see Ref. 33], if $K\sim 0.5$ the Coulomb-gap model should fail for $T_0/T<4$. This is in reasonable agreement with our observed limit of $T_0/T=2$–6 (see Fig. 3). We did not observe $p=\frac{1}{2}$ behavior for sample 1. Castner[32] suggested that for high doping density $T_0'/T_0\approx 80$. Given the measured T_0' for sample 1, we do not expect to see $p=\frac{1}{2}$ behavior for $T>0.06$ K.

A similar transition from Coulomb gap to Mott behavior has also been reported for 40–50 % compensated CdSe.[34] However, it is not clear that we should expect to see a transition to $p=\frac{1}{4}$ in any of these samples with $K\sim 0.5$. Shklovskii and Efros point out that at this compensation, the Coulomb gap extends over the entire range of impurity state energies, and there should be no temperature regime that satisfies the Mott approximation that the DOS is approximately constant for an energy range around the Fermi level comparable to the typical hopping energy (Ref. 13, p. 233).

Another reason that we are cautious about interpreting our data at high temperature is that the depth profiles of our implants are not rectangular (cf. Fig. 1). The more lightly doped wings of the profile should cause a downward curvature relative to the Coulomb-gap model prediction in both the high- and low-temperature regions, if the layers with different doping density independently show $(T_0/T)^{1/2}$ behavior with different T_0's. We have modeled the behavior expected in this case and find that while there is some change in the curvature of the models at high temperatures, the qualitative conclusions above are not affected.

Following the usual practice in experimental papers on hopping conduction, we have assumed so far that the preexponential factor ρ_0 in Eq. (1) is independent of the

temperature. Hopping theories generally predict that $\rho_0(T)=\rho_0 T^s$, where s is poorly determined but ≤ 1. When $\exp(T_0/T)^p$ is small, the temperature dependence of $\rho_0(T)$ may become important. Taking $s=2p$,[35] we refit the data with $\rho=\rho_0 T\exp(T_0/T)^{1/2}$. The resulting T_0 values were greatly increased, and the temperature range that could be approximately fit with $p=\frac{1}{2}$ was shifted to lower temperatures. However, the systematic deviations in the flat portions of the fit were significantly worse than those shown in Fig. 4. We see no particular justification in the data for including this term, although it cannot be ruled out.

V. SUMMARY

The Coulomb-gap model $\rho=\rho_0\exp(T_0/T)^{1/2}$ fits the data from our ion-implanted Si:P,B samples to high precision over a temperature range of $6.5<T_0/T<24$. The high-temperature limit of this range for the applicability of the Coulomb-gap model agrees with Castner's criterion for the temperature at which the mean hopping energy becomes comparable to the Coulomb-gap width. At low temperatures, the resistivity consistently increases more steeply than $p=\frac{1}{2}$, which could be due either to the onset of finite-thickness effects or to the creation of a hard gap by magnetic correlation effects.

ACKNOWLEDGMENTS

We thank M. Devlin, B. Edwards, C. Fassnacht, D. Henry, C. Hess, M.-T. Lin, E. Marietta, B. Mott, R. Pernick, C. Sappington, and D. Steffensrud for their assistance with device fabrication, testing, and construction of the adiabatic demagnetization refrigerator. We are particularly grateful to Henry Guckel and his students for their assistance with the detector processing development at the Wisconsin Center for Applied Microelectronics. We thank B. I. Shklovskii for many useful discussions. This work was supported in part by NASA Grants Nos. NAG5-679 and NAG5-594.

APPENDIX: THERMISTOR PROCESSING SEQUENCE

(1) Grow ~1-μm-thick SiO_2 on wafer surface in a 1040 °C furnace with 90 °C steam flow for 300 min followed by N_2 flow for 60 min.

(2) Pattern SiO_2 with buffered HF for degenerate electrical contact mask.

(3) Ion implant degenerate contact doping.

(4) Anneal implant at 980 °C with N_2 flow for 60 min.

(5) Pattern SiO_2 with buffered HF for thermistor implant mask.

(6) Ion implant thermistor doping.

(7) Remove SiO_2 from wafer with buffered HF.

(8) Anneal thermistor implant and grow ~200-Å oxide at 900 °C with 90 °C steam flow for 20 min followed by N_2 flow for 30 min.

(9) Pattern SiO_2 over degenerate contact implant for metalization.

(10) Sputter-deposit ~0.6-μm aluminum.

(11) Anneal aluminum metalization in 90% N_2/10% H_2 flow at 470 °C for 30 min.

(12) Pattern aluminum for an etch mask along the sides of the thermistor with $H_3PO_4/HNO_3/CH_3COOH$.

(13) Reactive ion etch the edges of the thermistors with NF_3 plasma at 100 W.

(14) Pattern aluminum for bonding pads with $H_3PO_4/HNO_3/CH_3COOH$.

[1]J. C. Mather, Appl. Opt. **21**, 1125 (1982).
[2]J. C. Mather, Appl. Opt. **23**, 584 (1984).
[3]J. C. Mather, Appl. Opt. **23**, 3181 (1984).
[4]S. H. Moseley, J. C. Mather, and D. McCammon, J. Appl. Phys. **56**, 1257 (1984).
[5]F. J. Low, J. Opt. Soc. Am. **51**, 1300 (1961).
[6]P. M. Downey, A. D. Jeffries, S. S. Meyer, R. Weiss, F. J. Bachner, J. P. Donnelly, W. T. Lindley, R. W. Mountain, and D. J. Silversmith, Appl. Opt. **23**, 910 (1984).
[7]D. McCammon, W. Cui, M. Juda, P. Plucinsky, J. Zhang, R. L. Kelley, S. S. Holt, G. M. Madejski, S. H. Moseley, and A. E. Szymkowiak, Nucl. Phys. A **527**, 821C (1991).
[8]D. McCammon, B. Edwards, M. Juda, P. Plucinsky, J. Zhang, R. L. Kelley, S. Holt, G. Madejski, S. H. Moseley, and A. E. Szymkowiak, in *Low Temperature Detectors for Neutrinos and Dark Matter III,* edited by L. Brogiato, D. V. Camin, and E. Fiorini (edition Frontiers, Gif sur Yvette, 1990), p. 213.
[9]J. Zhang, W. Cui, M. Juda, D. McCammon, R. L. Kelley, S. H. Moseley, C. K. Stahle, and A. E. Szymkowiak (unpublished).
[10]A. L. Efros and B. I. Shklovskii, J. Phys. C **8**, L49 (1975).
[11]A. Miller and E. Abrahams, Phys. Rev. **120**, 745 (1960).
[12]N. F. Mott, J. Non-Cryst. Solids **1**, 1 (1968).
[13]B. I. Shklovskii and A. L. Efros, in *Electronic Properties of Doped Semiconductors* (Springer-Verlag, Berlin, 1984).
[14]E. M. Hamilton, Philos. Mag. **26**, 1043 (1972).
[15]F. R. Allen and C. J. Adkins, Philos. Mag. **26**, 1027 (1972).
[16]A. N. Ionov, I. S. Shlimak, and M. N. Matveev, Solid State Commun. **47**, 763 (1983).
[17]A. G. Zabrodskii and K. N. Zino'eva, Pis'ma Zh. Eksp. Teor. Fiz. **37**, 369 (1983) [JETP Lett. **37**, 436 (1983)].
[18]A. G. Zabrodskii and K. N. Zino'eva, Zh. Eksp. Teor. Fiz. **86**, 727 (1984) [Sov. Phys. JETP **59**, 425 (1984)].
[19]Ning Wang, F. C. Wellstood, B. Sadoulet, E. E. Haller, and J. Beeman, Phys. Rev. B **41**, 3761 (1990).
[20]S. M. Grannan, A. E. Lange, E. E. Haller, and J. W. Beeman, Phys. Rev. B **45**, 4516 (1992).
[21]T. F. Rosenbaum, K. Andres, and G. A. Thomas, Solid State Commun. **35**, 663 (1980).
[22]S. Kobayashi, Y. Monden, and W. Sasaki, Solid State Commun. **30**, 661 (1979).
[23]W. N. Shafarman, D. W. Koon, and T. G. Castner, Phys. Rev. B **40**, 1216 (1989).
[24]J. C. Bourgoin, G. Frossati, A. Ravex, D. Thoulouze, M. Vandorpe, and B. Waksmann, Phys. Status Solidi B **92**, 585 (1979).
[25]C. C. Zammit and A. D. Caplin, Physica B **165&166**, 317

(1990).
[26]A. N. Ionov, M. N. Matveev, R. Rentzsch, and I. S. Shlimak, Pis'ma Zh. Eksp. Teor. Fiz. **42**, 330 (1985) [JETP Lett. **42**, 406 (1985)].
[27]W. Sasaki, Philos. Mag. B **52**, 427 (1985).
[28]B. I. Shklovskii (private communication).
[29]I. S. Shlimak, in *Hopping and Related Phenomena,* edited by H. Fritzsche and M. Pollak (World Scientific, Singapore, 1990), p. 49.
[30]R. W. van der Heijden, G. Chen, A. T. A. M. de Waele, H. M. Gijsman, and F. P. B. Tielen, Solid State Commun. **78**, 5 (1991).
[31]Peihua Dai, Youzhu Zhang, and M. P. Sarachik, Phys. Rev. Lett. **69**, 1804 (1992).
[32]T. G. Castner, in *Hopping Transport in Solids,* edited by M. Pollak and B. I. Shklovskii (North-Holland, Amsterdam, 1991), p. 1.
[33]M. Pollak and M. Ortuño, in *Electron-Electron Interactions in Disordered Systems,* edited by A. L. Efros and M. Pollak (North-Holland, Amsterdam, 1985), p. 287.
[34]Youzhu Zhang, Peihua Dai, Miguel Levy, and M. P. Sarachik, Phys. Rev. Lett. **64**, 2687 (1990).
[35]R. Mansfield, Philos. Mag. B **57**, 777 (1988).